Biophysical Chemistry, 49 (1994) 113–126
Elsevier Science B.V., Amsterdam

BIOCHE 1804

Tryptophan photophysics in rabbit skeletal myosin rod

Yoke-chen Chang and Richard D. Ludescher *

Department of Food Science, Rutgers University and the New Jersey Agricultural Experiment Station, Cook College, New Brunswick, New Jersey 08903, USA

(Received 18 May 1993; accepted in revised form 18 August 1993)

Abstract

The fibrous region of myosin (myosin rod) is an α-helical, two-stranded coiled-coil made up of identical chains of nearly 1000 residues. Myosin from rabbit skeletal muscle has two tryptophans per chain located at identical hydrophobic *d* sites in the heptad repeat that forms the basis for hydrophobic dimerization. The fluorescence excitation and emission spectra of rod in high salt buffer (where the rod exists as a coiled-coil monomer) at 20°C are red- and blue-shifted, respectively, from the comparable spectra of *N*-acetyl-tryptophanamide or L-tryptophan. These spectral shifts, as well as red-shifts in the emission spectra induced by excitation on the red edge of the absorption or by increases in temperature, indicate that (on average) the tryptophans are partially exposed to aqueous solvent yet in contact with the protein matrix. The tryptophan intensity decays show an unusual bimodal distribution; the major species has a discrete lifetime of about 5.2 ns while the minor species exhibits a complex decay with a broad (3.4 ns full width at half maximum) Gaussian distribution of lifetimes centered around 1.3 ns. The long lifetime species has a blue-shifted excitation and red-shifted emission characteristic of the indole chromophore in a polar (probably aqueous) environment while the short lifetime species has the spectral parameters characteristic of indole in a non-polar environment. Although assignment of these lifetime species to particular tryptophans in the rod is problematic, this study indicates that the coiled-coil interface presents a complex heterogeneous environment that may undergo rapid conformational mobility.

Keywords: Fluorescence; Lifetimes; Coiled-coil; Tryptophan; Myosin rod

1. Introduction

The α-helical coiled-coil, the supersecondary structural element formed from the supercoiling of two α-helical segments, is an important structural motif in proteins [1,2]. It forms a major structural element in myosin [3], in tropomyosin [4], in the intermediate filaments of the cellular cytoskeleton (5), and in a class of dimeric DNA binding proteins that regulate gene expression

* *Correspondence to*: Dr. Richard Ludescher, Dept. of Food Science, P.O. Box 231, Cook College, New Brunswick, NJ 08903-0231.

Abbreviations: EDTA, ethylenediaminetetraacetic acid; FWHM, full width half maximum; MB, myosin buffer; KDP, potassium dihydrogen phosphate; LMM, light meromyosin; MOPS, 4-morpholinepropanesulfonic acid; NATA, *N*-acetyl-tryptophanamide; NdYAG, neodymium yttrium aluminum garnet; SDS, sodium dodecyl sulfate; S-1, subfragment 1; S-2, subfragment 2.

Elsevier Science B.V.
SSDI 0301-4622(93)E0058-D

(the so-called leucine zipper proteins) [6]. The structural interactions between α-helices that generate the coiled-coil also form the basis of significant folding interactions in many globular and intrinsic membrane proteins [2].

The coiled-coil is a dimer of α-helical polypeptides twisted together into a left-handed supercoiled rope [4]. The dimerization interface is a hydrophobic surface composed of non-polar side chains that arises from a periodic seven-residue, or heptad, repeat, $(abcdefg)_n$, where the first (a) and fourth (d) residues are non-polar and the remaining residues are predominately polar. Ionic interactions between oppositely charged residues at the e and g sites further stabilize the coiled-coil. The apolar residues, which form a left-handed helical stripe on the α-helix surface, pack together in a "knobs into holes" format when the long axes of two helices are aligned at $\approx 18°$ to one another [4,7]. The long pitch of the left-handed coiled-coil is about 14 nm. Most coiled-coil proteins, including myosin, are dimers of identical subunits with polypeptide chains parallel and in axial register.

Particular amino acids are known to favor specific sites within the coiled-coil [8]. Leucine, for example, occurs frequently at a and d sites, while tryptophan is uncommon throughout coiled-coils. The research reported here exploits the relative rarity of tryptophan in coiled-coils in order to probe the local structure and conformation at specific sites in myosin rod, the coiled-coil region of myosin.

Coiled-coil fibrous proteins are often a mixture of globular and coiled-coil domains. The heavy chains of muscle and cytoplasmic myosin II are representative examples. Myosin heavy chains are large polypeptides (220 kD) with about 1950 amino acids [9]. About 850 residues at the N-terminus fold into a globular head that contains the ATPase and actin binding sites; the remainder of the protein is a nearly continuous stretch of α-helical coiled-coil about 160 nm long and 2 nm in diameter [3]. This fibrous region aggregates at physiological salt concentrations to form the thick filaments of muscle [10]. Sequences of the coiled-coil tail from several vertebrate myosins including rabbit skeletal are known [11,12]. There are two tryptophans per heavy chain, conserved in all known vertebrate skeletal myosins, that are located at hydrophobic d sites in the heptad repeat (there are no tryptophans in the coiled-coil regions of smooth muscle or non-muscle myosin, or in tropomyosin).

In addition to its structural function in the formation of the thick filament, the coiled-coil region of myosin performs several possible dynamic functions in the mechanism of muscle contraction. Flexibility in the fibrous region of the thick filament crossbridge, either within subfragment-2 (S-2) or at the junction between S-2 and LMM, facilitates proper orientation of the myosin head with respect to the actin filament [13]. By connecting the actin-bound head to the thick filament, the coiled-coil of myosin couples the force generated by the head to vectorial motion of the overlapping thick and thin filaments. Additional functions have been postulated but remain moot. The fibrous tail may, for example, store tension during the intervals between force-generation and the relative vectorial movement of the filaments [14]; this last function may be inextricably associated with the mechanical function of coupling force to movement.

Myosin can be digested at the head–tail junction by α-chymotrypsin in the absence of Mg^{2+} [15]. The fibrous fragment, myosin rod, contains the two pairs of tryptophan residues [16] which are located near the N-terminal of the LMM fragment near the S-2 junction [12]. We are using fluorescence from these residues to probe the structure and local conformation of the coiled-coil in myosin; this work thus expands upon previous steady-state studies using tryptophan fluorescence to monitor thermal transitions in the rod [16]. We characterize here the steady-state and time-resolved photophysical behavior of these tryptophans; preliminary descriptions of this work have been reported elsewhere [17,18].

2. Materials and methods

2.1. Protein preparations

Myosin was extracted from the skeletal muscle of New Zealand white rabbits. Myofibrils were

prepared from the minced leg and back muscle [19] and myosin was isolated from the crude myofibrils [20]. The purified myosin was stored at −20°C in myosin buffer (MB: 0.5 *M* KCl, 0.5 m*M* EDTA, 0.5 m*M* dithiothreitol, 20 m*M* MOPS, pH 7.0) that contains 50% glycerol (v/v) as an antifreeze. The myosin rod was prepared from myosin by digestion with α-chymotrypsin (Sigma Chemical Co., St. Louis, MO) at room temperature at low ionic strength in the absence of Mg^{2+} (0.12 *M* KCl, 20 m*M* MOPS, 1 m*M* EDTA, pH 7.0) according to published methods [15]. The myosin rod was purified from S-1 and undigested myosin by ethanol precipitation [21]. The purity of rod samples was checked by SDS-polyacrylamide gel electrophoresis [20]. The three rod preparations that were used to collect the data cited herein all showed one dominant band in 10% polyacrylamide gels. Densitometry of stained gels indicated that the protein was ≥ 95% rod with the remainder smaller fragments. The purified myosin rod was stored at −20°C in MB plus 50% glycerol (as described above).

2.2. Steady-state spectroscopic measurements

All steady-state fluorescence spectra, intensity and polarization measurements were made on a SPEX model F1T11 spectrofluorimeter (SPEX Industries, Metuchen, NJ) equipped with Glan–Thompson polarization optics; the temperature of the sample holder was controlled by a water bath.

Excitation and emission spectra were typically collected with 1.9 nm bandpass resolution using emission at 350 nm and excitation at 290 nm. Emission spectra were also collected using excitation at 275, 280, 290, 295, 300 and 305 nm with 1.9 nm bandpass. Difference spectra were collected by subtracting the emission spectrum with excitation at 295 nm from the emission spectra with excitation at 275, 280 and 290 nm; the spectra were normalized to equal intensity at long wavelengths (360 nm). Emission spectra with excitation at 280 nm (bandpass 1.9 nm) were collected as a function of temperature at 0, 10, 20, 30 and 39.4°C after a 15 minute equilibration time; the temperature was measured in the cuvette using a thermocouple detector.

The relative fluorescence quantum yield of myosin rod was calculated as the ratio of the area under the rod uncorrected emission spectrum to the comparable area under the L-tryptophan uncorrected emission spectrum collected in pH 6.0 buffer at 20°C under identical instrumental conditions (the quantum yield is 0.12 for tryptophan under these conditions; [22]); the ratio was adjusted to account for any differences in absorption.

The fluorescence excitation and emission anisotropy spectra were collected as the raw polarization spectra VV, VH, HV, and HH (where the first letter indicates the polarization direction of the excitation and the second letter the emission); comparable spectra of the buffer (background) were subtracted from each spectrum. Excitation anisotropy spectra with 0.94 nm bandwidth resolution were collected with emission at 360 nm (30 nm bandwidth); emission anisotropy spectra with 7.5 nm bandwidth resolution were collected with excitation at 300 nm (7.5 nm bandwidth). The steady-state fluorescence anisotropy, $\bar{r}$, was calculated from the raw polarization spectra using the equations $\bar{r} = (R-1)/(R+2)$, where $R = (\mathrm{HH} \times \mathrm{VV})/(\mathrm{HV} \times \mathrm{VH})$.

The protein and NATA concentrations were 1–10 μ*M* for all anisotropy and spectral measurements and were adjusted to keep the absorbance at the excitation wavelength ≤ 0.05 to avoid inner filter effects [23].

2.3. Time-resolved spectroscopic measurements

Fluorescence decay measurements were performed on the time-correlated single photon counting fluorimeter at the Regional Laser and Biotechnology Laboratory (RLBL), Department of Chemistry, University of Pennsylvania. This instrument uses as a light source the doubled output of a Coherent Antares mode-locked NdYAG laser pumping a dye laser. The red dye laser output from rhodamine 6G, cavity dumped at 4 MHz, was doubled in a KDP crystal to an excitation wavelength in the range from 280–300 nm. Instrument response functions, generated by

scattering excitation light from a solution of coffee creamer, and total intensity decays from myosin rod emission were collected using magic angle polarization following vertically polarized excitation. This instrument uses a Hamamatsu microchannel plate detector; typical instrument response curves had a FWHM of less than 100 ps. The lifetime decays were collected as a function of emission wavelength at 315, 330, 345, 360, 375 and 390 nm (bandwidth 10 nm) with excitation at 290 nm using an American Holographic DB-10 double monochromator operating in subtraction mode.

The lifetime decays were fit to a sum of exponentials using a non-linear least squares iterative reconvolution program developed by Dr. Gary Holtom at the RLBL. The relevant equation was:

$$I(t) = I_0 \sum_{i=1}^{n} a_i \, e^{-t/\tau_i} \qquad (1)$$

where I_0 is the initial (maximum) value of the decay, and a_i is the normalized amplitude and τ_i the lifetime of component i. The goodness-of-fit for a particular decay model was evaluated by examination of the magnitude of χ^2 for fits with various lifetime components (various values of n in the above equation) and by examination of a plot of the modified residuals (the difference between the calculated and experimental decay values divided by the square root of the experimental value). A fit was considered appropriate when the modified residuals showed random deviations about zero and the χ^2 was in the range 1–1.2.

The fluorescence decay curves collected as a function of emission wavelength were also analyzed using global fitting procedures [24]. This approach is based on the principle that simultaneous analysis of multiple data sets will effectively over-determine the estimation problem and improve the reliability of the fit parameters. Three independent sets of lifetime decays collected as a function of emission wavelength (315, 330, 345, 360, 375, and 390 nm) were fit to various decay models (described in Results) using the program Globals Unlimited (University of Illinois) developed by Beechem and colleagues [24]. This global analysis program allows the lifetime decays at all emission wavelengths to be analyzed simultaneously by linking the amplitude and lifetime parameters across data sets and varying only the lifetime amplitudes, only the lifetimes, or both sets of parameters. The goodness-of-fit for each decay analysis was evaluated by calculating χ^2 and by examining plots of the modified residuals and autocorrelation function of the residuals [25]. A fit was considered proper when the global χ^2 was lower than 3.0 and the modified residuals and its autocorrelation function showed random deviations about zero. The data sets were analyzed using probability density functions that assumed different possible models for the lifetime distributions; these included multiple discrete lifetimes, and distributions of lifetimes with Lorentzian and Gaussian shapes. The use of distribution models is based on statistical mechanical analyses of the effect of protein dynamics on fluorophore lifetimes [26,27] and on previous experimental findings [28].

3. Results

3.1. Steady-state fluorescence spectra

The tryptophan fluorescence of myosin rod in high salt myosin buffer at 20°C had an excitation maximum at 279 nm and an emission maximum at 340 nm (Table 1). These values were shifted

Table 1

Fluorescence spectral parameters of myosin rod and model compounds [a]

Sample	Excitation		Emission		Quantum Yield [d]
	Maximum [b] (nm)	FWHM (nm)	Maximum [c] (nm)	FWHM (nm)	
L-Tryptophan	278	34	356	68	0.12
NATA	278	34	357	68	–
Myosin Rod	279	32	340	61	0.11

[a] All data collected at 20°C from samples in MB.
[b] Emission at 350 nm.
[c] Excitation at 290 nm.
[d] Quantum yield based on 0.12 for L-tryptophan at pH 6.0 [22].

from the excitation and emission maxima for L-tryptophan amino acid (278 nm and 356 nm) and NATA (278 nm and 357 nm) measured under identical solution conditions (Table 1). Although red-shifts in the excitation and blue-shifts in the emission spectra of the indole chromophore of tryptophan are associated with transfer to a non-polar medium [29], the value of the emission maximum for rod suggests that the tryptophans are on average in partial contact with aqueous solvent. The bandwidths (FWHM; full width at half maximum intensity) of the excitation and emission spectra of the tryptophans in rod were also significantly narrower, 32 nm and 61 nm, respectively, than the comparable bandwidths of 34 nm and 68 nm seen in L-tryptophan and NATA (Table 1). Again, although narrow bandwidths of tryptophan spectra are associated with non-polar environments [30] the width of these spectra suggest that, despite the location of the tryptophans at hydrophobic *d* sites in the rod, the indole rings are actually in partial contact with solvent.

There are five tyrosines per polypeptide chain in the rod at relative positions 508, 621, 649, 1011 and 1037. The positions of the two tryptophans per chain are indicated in Fig. 1; they are located at positions 532 and 617 (numbering system of ref. [12]). Although the emission spectrum of rod with excitation at 280 nm showed no obvious indications of tyrosine emission, difference spectra were collected to confirm this point. Emission spectra of rod with excitation at 275, 280, and 290 nm were compared with a spectrum excited at 295 nm, a wavelength region in which the tyrosine absorbance is negligible [23,31,32]. The difference spectra with excitation at 275 nm (the maximum of the tyrosine absorbance) and at 280 nm revealed a weak emission band with a peak near 305 nm and a tail extending out to about 360 nm (spectra not shown); this band amounted to less than 5% of the total integrated emission intensity. The difference spectrum with 290 nm excitation, however, was flat and random about zero intensity; this indicated that there was no tyrosine fluorescence from the rod with excitation at 290 nm. A similar result was found by Cowgill [33].

Both the fluorescence excitation and emission spectral maxima of rod were dependent upon other spectral parameters. The wavelength of the fluorescence excitation peak blue-shifted slightly to shorter wavelength as the emission position was moved to longer wavelength; the excitation maxima were 281 nm with 315 nm emission and 279 nm with 390 nm emission. The wavelength of the fluorescence emission peak, on the other hand, red-shifted slightly to longer wavelength as the excitation position was moved to longer wavelength; the emission maxima were 340 nm with 280 nm excitation and 342 nm with 305 nm excitation. Such red-shifts in emission spectra with

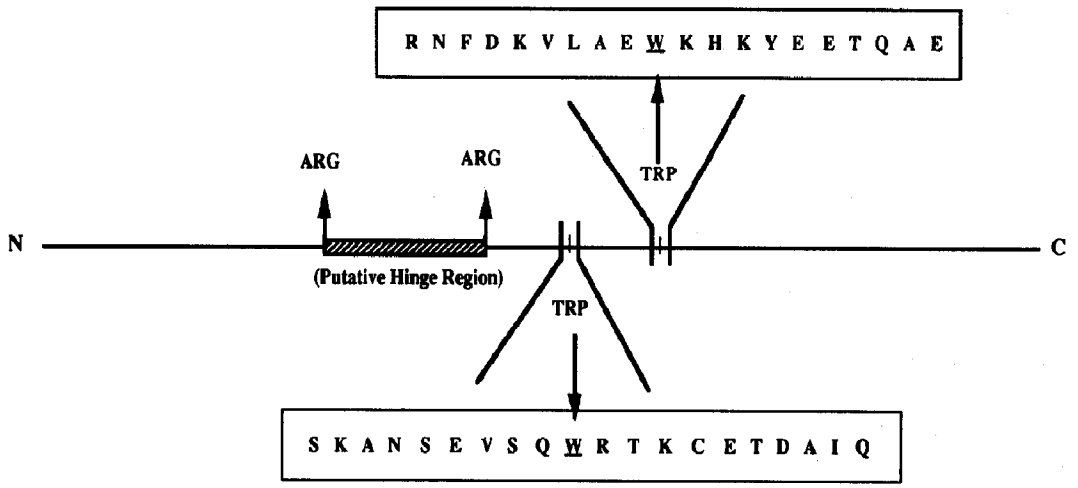

Fig. 1. Schematic structure of rabbit skeletal myosin rod indicating the relative positions of the two pairs of tryptophans and the amino acid sequence around each tryptophan residue.

excitation at the red-edge of the absorption spectra are suggestive of slow ($\leq$ ns) solvent dielectric relaxation around the polar tryptophan excited state [34,35]. The emission spectra of tryptophan in the rod were also influenced slightly by temperature; the emission maximum shifted from 340 nm at 0°C and 20°C to 341 nm at 39.4°C (the rabbit body temperature); this result agrees with a previous, and more detailed, fluorescence study of thermal unfolding in the rod [16]. Since the rod helix containing the two tryptophans melts above about 47°C [16,36,37], these spectral shifts probably reflect an increase in solvent dielectric relaxation with temperature rather than protein structural changes such as unfolding [38–40].

3.2. Steady-state polarization

The variation across both the excitation and emission bands of the steady-state anisotropy of rod in MB at 20°C are shown in Fig. 2B. The excitation anisotropy shows the complex wavelength dependence characteristic of the overlapping ^1L_a and ^1L_b transitions in tryptophan [41]. The anisotropy leveled off at a constant high value of 0.20 at wavelengths $\geq$ 300 nm; our value of the anisotropy at 297 nm excitation is essentially identical to that found by King and Lehrer [16]. The maximum (no motion) value of the steady-state anisotropy (r_0) for tryptophan in our instrument was $\approx$ 0.30 at 300 nm; this value was estimated from the polarization of NATA in glycerol at −12°C (Fig. 2A). An anisotropy value of 0.20 at 300 nm thus indicates that the side chains of the four tryptophans in rod are, on average, mobile but restricted in angular motion on the time scale of the fluorescence lifetime (about 4.5 ns, see below). Such mobility suggests that the indole side chains are not significantly constrained by the protein matrix of the rod; this mobility is consistent with the extent of solvent exposure suggested by the peak position and band width of the emission spectrum.

The emission anisotropy of both the rod (in MB at 20°C) and NATA (in glycerol at −12°C) decreased as a function of increasing emission wavelength (Fig. 2). Comparable decreases in polarization with increasing emission wavelength are

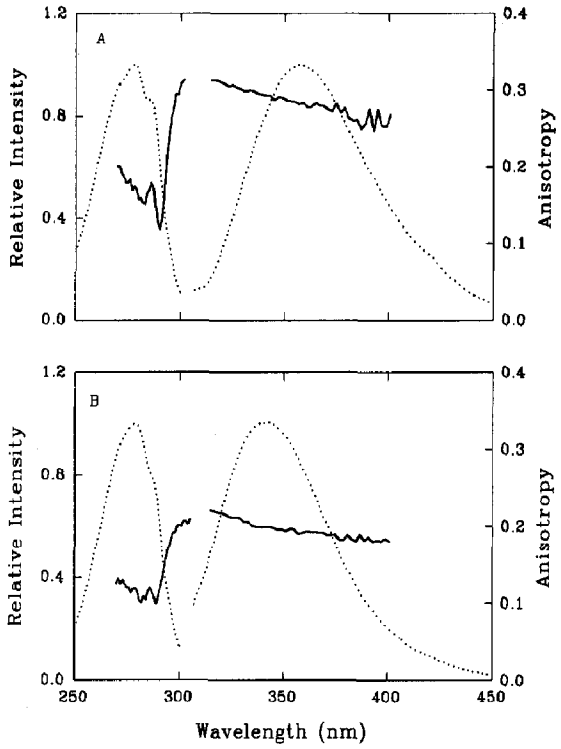

Fig. 2. Excitation and emission polarization anisotropy (solid curves) and normalized intensity (dotted curves) spectra of (A) *N*-acetyl tryptophanamide in 100% glycerol at −12°C and (B) myosin rod in MB at 20°C.

seen in L-tryptophan amino acid and model compounds as well as in a number of proteins containing both single and multiple tryptophans [42,43] suggesting that the decrease is an intrinsic property of the indole chromophore. The decrease was linear with increasing wavelength for NATA. In the case of the tryptophans in the rod, however, the decrease was biphasic; the slope of the wavelength dependence was steeper at short wavelengths ($\leq$ 340 nm) than at long wavelengths. This biphasic character suggested that there are at least two emitting species in the rod with different emission anisotropies and that the fractional fluorescence from these species changed with wavelength.

3.3. Time-resolved fluorescence

A fluorescence intensity decay curve of the tryptophan emission from myosin rod in MB at 20°C is plotted in Fig. 3A along with modified

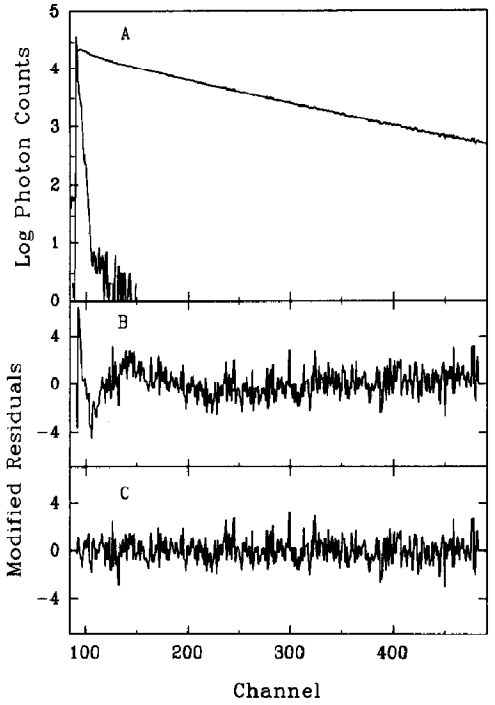

Fig. 3. Time-resolved intensity decay of tryptophan fluorescence from myosin rod at 20°C in MB. Excitation at 290 nm and emission at 315 nm (10 nm bandwidth). (A) Log of photon counts versus channel number (channel resolution of 46.7 ps/channel) for unconvoluted total intensity decay and instrument response function. Modified residuals for discrete two (B) and three (C) component lifetime analyses (fit parameters are tabulated in Table 2).

Table 2

Discrete exponential analyses of tryptophan fluorescence from myosin rod [a]

n [b]	Fit parameters						χ^2
	a_1	τ_1 (ns)	a_2	τ_2 (ns)	a_3	τ_3 (ns)	
2	0.71	5.07	0.29	0.87			1.72
	0.01 [c]	0.03	0.01	0.05			
3	0.60	5.18	0.19	1.49	0.21	0.25	1.06
	0.01	0.04	0.01	0.07	0.01	0.02	

[a] Data collected at 20°C in MB using 290 nm excitation and 315 nm emission.

[b] A single data set was fit to eq (1) (see Section 2) using $n = 2$ or $n = 3$.

[c] Standard deviations calculated from comparison of the fit values to at least three data sets.

residuals plots for discrete two (Fig. 3B) and three (Fig. 3C) exponential fits. The fit parameters for analyses of the intensity decay using two or three exponentials are tabulated in Table 2. Under these conditions of excitation (290 nm) and emission (315 nm) the decay appeared triple exponential: plots of the modified residuals were flat and random about zero for three (Fig. 3C) but not two components (Fig. 3B) and the χ^2 value was close to unity (Table 2).

The fluorescence intensity decays of myosin rod varied as a function of both excitation and emission wavelength; the normalized amplitudes and lifetimes from discrete multi-exponential analyses of individual decays are plotted versus

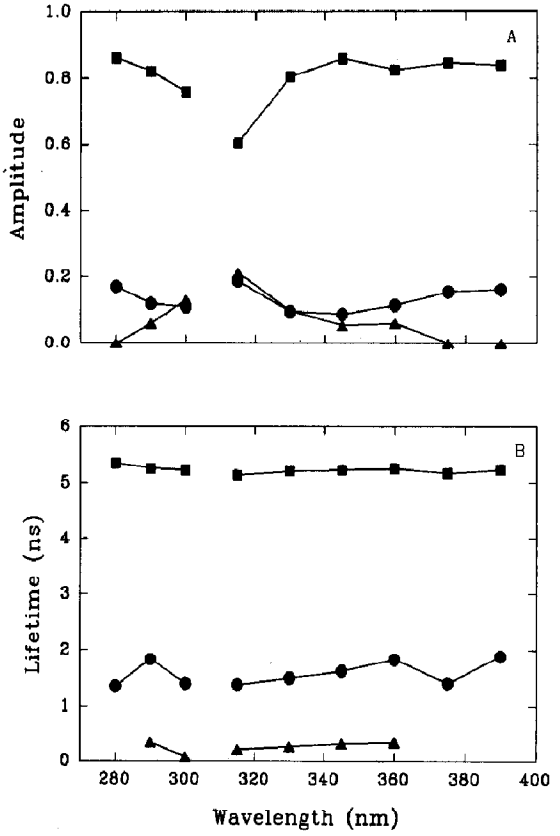

Fig. 4. Excitation and emission wavelength dependence of the normalized amplitudes (A) and lifetimes (B) of tryptophan fluorescence from myosin rod at 20°C in MB. The solid symbols are the fit amplitude and lifetime values for the long (■), intermediate (●), and short (▲) lifetime components from discrete multi-exponential analyses (eq. 1, Section 2) of individual data sets collected at the indicated wavelengths.

wavelength in Fig. 4. The data were well fit with three exponentials at all but short excitation (280 nm) and long emission wavelengths ($\geq$ 375 nm) where the decays were well fit with two exponentials. The lifetime components of approximately 0.3 ns, 1.6 ns, and 5.2 ns were essentially constant across both the excitation and emission bands (Fig. 4B) indicating that the same three fluorescence species were contributing to these decays at all wavelengths; there was thus no evidence for tyrosine emission in the time-resolved intensity decays at short wavelengths.

The normalized amplitudes, however, varied with wavelength (Fig. 4A). The amplitude of the long lifetime component increased with emission wavelength from a low of 0.6 at 315 nm to about 0.8 at 345 nm and above; there was a concomitant decrease in the amplitude of the short (0.3 ns) lifetime component over the same wavelength range. The excitation dependence of the lifetime amplitudes, however, showed a different trend; the amplitude of the long lifetime component decreased with excitation wavelength from a value of 0.83 at 280 nm to 0.76 at 300 nm while the amplitude of the short lifetime component increased over the same wavelength range (Fig. 4A). This constancy of lifetimes and systematic changes in lifetime amplitudes over both the excitation and emission bands is consistent with an association of lifetimes with distinct excitation and emission spectra that has been seen in several other proteins [44–46].

The fluorescence intensity decays collected as a function of emission wavelength were also analyzed using global fitting procedures [24] in which the lifetimes used to describe multiple data sets at different emission wavelengths were linked (constrained to the same value for all decays) while the amplitudes were allowed to vary for each decay. Independent sets of six emission decays collected at 315, 330, 345, 360, 375, and 390 nm (10 nm bandwidth) were fit using global analysis methods to four different decay models: a discrete two-exponential, a discrete three-exponential, a bimodal Lorentzian distribution, and a bimodal Gaussian distribution.

The discrete two exponential global analyses gave poor fits to the data with global χ^2 values in the range from 5–6; modified residuals plots for the data at short wavelengths resembled those for the double exponential fit plotted in Fig. 3B. Discrete three exponential analyses, however, gave good fits to all data sets with global χ^2 values in the range from 2.3–3.8 and flat and

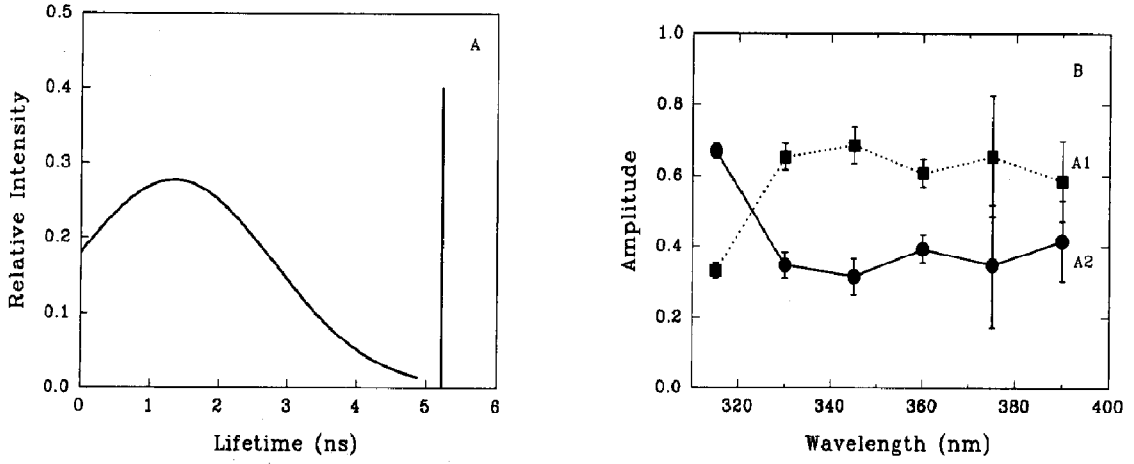

Fig. 5. Parameters from global analysis of tryptophan total intensity decays for myosin rod at 20°C in MB collected as a function of emission wavelength (10 nm bandwidth). Three independent data sets were analyzed using a Gaussian bimodal distribution with lifetimes linked and amplitudes variable across data sets. (A) Bimodal distribution of lifetimes that describes all data sets. The long lifetime distribution has a mean of 5.22 ns and FWHM of 0.001 ns and the short lifetime distribution has a mean of 1.34 ns and FWHM of 3.4 ns. (B) Normalized amplitudes of long (■) and short (●) lifetime distributions plotted versus emission wavelength. The error bars represent standard deviations from analyses of three independent data sets.

random residuals plots. The fit values of the linked lifetimes from these analyses, about 0.3, 2, and 5.2 ns, were similar to those found using analysis of individual decays (Fig. 4B). The wavelength dependence of the normalized amplitudes from these analyses were the same, within experimental error, to the amplitudes from the discrete analyses of individual data sets plotted in Fig. 4A except that the amplitude of the short (0.35 ns) lifetime component, although small, did not go to zero at long emission wavelengths. The intermediate and short lifetimes from these global analyses varied in the range from 2.6–1.7 ns and from 0.5–0.2 ns, however, depending on the particular value of the initial estimate of their lifetime; this behavior indicated that the discrete lifetime model did not give a unique fit to the data in spite of the additional, strong constraints provided by the global analysis procedure [24].

Analyses using a bimodal Lorentzian model gave very poor fits with global χ^2 values in the range from 9–10 and non-random residuals plots (data not shown). Analyses using a bimodal Gaussian distribution, however, gave excellent fits with global χ^2 values in the range from 2.7–3.1 and flat and random residuals plots for all data sets. A similar bimodal Gaussian analysis was required to fit the time-resolved fluorescence quenching of this protein by acrylamide or iodide [47]. The fit lifetime distributions from the bimodal Gaussian model are plotted in Fig. 5A. The long lifetime component was fit by a narrow (FWHM of 0.001 ns) Gaussian distribution with a mean of 5.22 ns; the analysis thus demonstrated that the long lifetime component was indeed a discrete lifetime. The short lifetime component(s), however, were fit by a broad (FWHM of 3.4 ns) Gaussian distribution of lifetimes centered around 1.34 ns. The amplitudes of the long and short lifetime distributions from the global analysis are plotted versus emission wavelength in Fig. 5B. The amplitude of the discrete long lifetime increased from 0.33 at 315 nm to ≈ 0.65 at wavelengths ≥ 330 nm; the amplitude of the Gaussian distribution of short lifetime species showed a corresponding decrease from 0.67 to 0.35 over the same wavelength range.

4. Discussion

4.1. Tyrosine emission

Although there are 10 tyrosines in the rod (five per heavy chain), there was very little emission from these residues upon excitation at their absorbance maximum of 275 nm and no emission detectable upon excitation at 290 nm in either the steady-state spectra or the time-resolved intensity decays. A similar conclusion was reached in an early study of fluorescence from LMM, the C-terminal fragment of the rod [33]. Two of these tyrosine residues, those at positions 508 and 621, are located within approximately 35 Å of one of the tryptophan residues (assuming a linear α-helical secondary structure within the rod and a rise/residue of 1.5 Å); since the R_0 for tyrosine to tryptophan energy transfer is in the range from 10–18 Å [32,48,49] these residues can, in principle, transfer excitation energy through a Förster process to tryptophan [23,50]. Such transfer could account for significant quenching of the fluorescence from these residues. The other three tyrosines, however, those at positions 649, 1011 and 1037, are too distant from a tryptophan (≈ 50 Å for Y649 and ≥ 500 Å for the others) to engage in energy transfer. Fluorescence from these tyrosines, as well as those near the tryptophans, may be quenched by interactions of the phenol side chains with other groups within the protein.

4.2. Average environment of the tryptophan residues

The tryptophan fluorescence from rod has an emission spectrum that is blue-shifted and narrower than the emission from either L-tryptophan or NATA in the same buffer. Since the fluorescence spectral properties of L-tryptophan and NATA in myosin buffer reflect the case of full solvent exposure of the indole ring, the emission spectral properties of the rod suggest that the tryptophans are only in partial contact with aqueous solvent; these residues may be classified as surface (type II) tryptophans according to the system of Burstein and colleagues [30]. Similar fluorescence properties have been seen in pro-

teins with single tryptophan residues such as phospholipase A_2 [28] where the tryptophan is known from crystallographic studies to be located at the protein surface with one face of the ring in contact with solvent. The red-shifts seen in the emission spectra upon red-edge excitation or increasing the temperature also suggest that some solvent dipolar relaxation occurs around the excited state of the tryptophans on a time scale comparable to fluorescence emission. Relaxation on the nanosecond time scale must reflect reorientations of a viscous protein matrix rather than a fluid aqueous solvent [40,51].

Sequence analysis of the rabbit myosin rod [12] indicates that the two tryptophans in each polypeptide chain are located at equivalent hydrophobic *d* sites at the coiled-coil sequence; their putative positions are indicated schematically in Fig. 6. The fluorescence properties of rod, however, suggest that the indole rings of these side chains are, on average, located near the surface of the coiled-coil in partial contact with aqueous solvent rather than buried at the hydrophobic interface between the helixes. The small red-shift of the excitation spectra of the rod compared to L-tryptophan or NATA is also consistent with this interpretation; the absorption spectra of indole or *N*-acetyl-tryptophan ethyl ester are red-shifted in a polar solvents with high polarizability and blue-shifted in polar solvents with low polarizability such as water [29].

4.3. Polarization

The emission anisotropy of myosin rod, like that of many other proteins [42,43], decreased

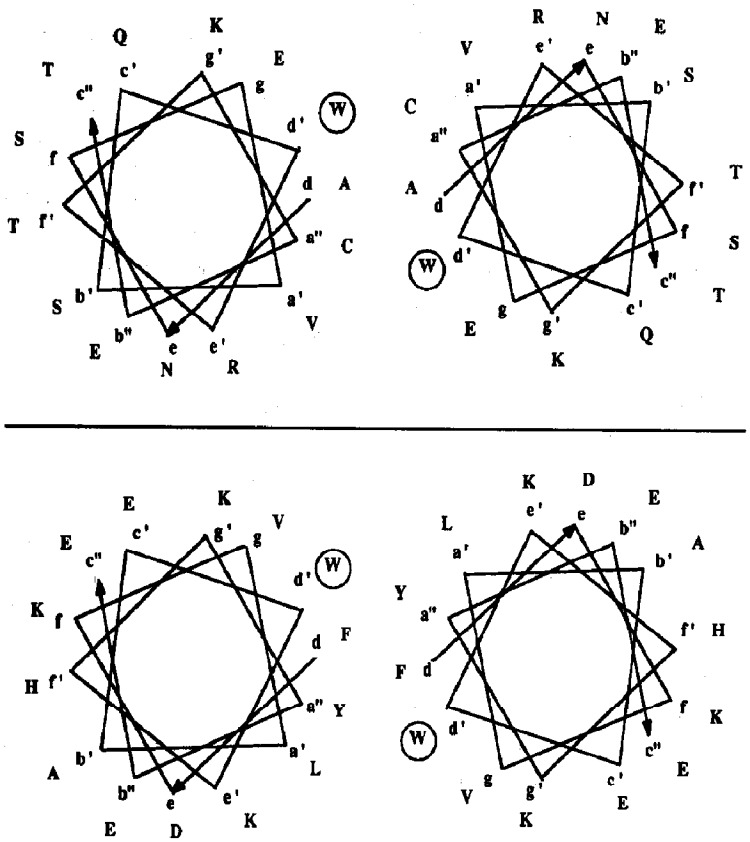

Fig. 6. Helix wheel representation of the putative coiled-coil conformation around the two pairs of tryptophans in rabbit skeletal myosin rod. (A) Conformation around the first tryptophan in the sequence (W532); (B) conformation around the second tryptophan in the sequence (W617).

with increasing emission wavelength. Unlike the linear decrease seen in NATA (Fig. 2A), however, the decrease in rod was biphasic suggesting that the anisotropy was the sum of emission from two (or more) species with different wavelength-dependent anisotropies. With two lifetime species, the measured anisotropy as a function of wavelength ($\bar{r}(\lambda_{em})$) will be the weighted sum of the anisotropies ($\bar{r}_i(\lambda_{em})$) from each species:

$$\bar{r}(\lambda_{em}) = f_1(\lambda_{em})\bar{r}_1(\lambda_{em}) + f_2(\lambda_{em})\bar{r}_2(\lambda_{em}) \quad (2)$$

where the $f_i(\lambda_{em})$ terms are the fractional fluorescence intensities as a function of emission wavelength [52] and the $\bar{r}_i(\lambda_{em})$ terms have a wavelength dependence similar to that of NATA in glycerol (Fig. 2A); the magnitude of the $\bar{r}_i(\lambda_{em})$ terms are sensitive to the rotational dynamics and the lifetime of each species [23]. Although it is not possible to calculate specific values for $\bar{r}_i(\lambda_{em})$ from our data (because each wavelength point represents a single equation with two unknowns), this interpretation does suggest that the wavelength dependence of the emission anisotropy reflects the wavelength dependence (Figs. 4A and 5B) of the different fluorescent species seen in the rod.

4.4. Tryptophan lifetimes

Despite the presence of four tryptophans in at least two chemically distinct environments in the rod (positions 532 and 617), the emission decays were dominated by a single, discrete, long lifetime species of about 5.2 ns that represented at least 60% and perhaps as much as 80% of the emitting chromophores. The remaining fluorescence exhibited complex, heterogeneous emission decay behavior that required either two discrete lifetimes (Table 2) or a broad Gaussian distribution of lifetimes (Fig. 5A) for an adequate description.

In spite of this complexity, we conclude that the fluorescence decay at short time in the rod reflects a broad Gaussian distribution of lifetimes for three reasons. First, the large variations observed in the final fit lifetime parameters upon changing the initial lifetime estimates in the global analyses indicated that the lifetime parameters were ill-defined in the discrete lifetime model; this suggested that the χ^2 surface characterizing the discrete fits to the short lifetime components had no well-defined minima in spite of the strong constraints provided by the global analysis. Second, a previous study of the quenching of the tryptophans in myosin rod by acylamide and iodide [47] demonstrated that a bimodal Gaussian distribution, but not a discrete lifetime, model could provide an adequate description of the time-resolved intensity decays collected as a function of quencher concentration. And, third, the bimodal Gaussian distribution model actually provided a simpler description of the data: a distribution model required only two parameters (mean and width of the distribution) to describe the complex decay behavior at short time while a discrete lifetime model required three parameters (two lifetimes and the fractional distribution between them).

The excitation and emission dependence of the lifetime amplitudes (Fig. 4A) indicated that the discrete long lifetime species was associated with the blue-shifted excitation and red-shifted emission spectra characteristic of an indole chromophore in contact with polar solvent. The short lifetime distribution, on the other hand, was associated with the red-shifted excitation and blue-shifted emission spectra characteristic of the indole chromophore in a non-polar environment. The general description of the tryptophan environment in the myosin rod outlined above on the basis of steady-state fluorescence must thus be modified. There are apparently two distinct fluorescent species in the rod. The major species with a discrete long lifetime is in a polar environment and thus, probably, near the surface of the coiled-coil and the minor species (possibly characterized by a broad distribution of lifetimes) is in a more non-polar environment and thus, probably, partially buried within the rod, perhaps at the coiled-coil interface. This interpretation is strongly supported by the time-resolved quenching study of myosin rod [47] which found that the long lifetime species is more readily quenched by acrylamide or iodide, and thus has a much higher

solvent accessibility [53], than the short lifetime species.

The association of the long, 5.2 ns, lifetime with a species of aqueous solvent-exposed tryptophans apparently runs counter to the findings of studies of the influence of solvent on the indole chromophore in model compounds [54] where contact with water was found to shorten the excited state lifetime. Studies of several proteins containing multiple tryptophans, however, indicate that the findings of these model studies may not be generalizable to proteins. The long lifetime component of tryptophan fluorescence has been associated with a red-shifted emission spectrum in the double tryptophan proteins lac repressor [44], horse liver alcohol dehydrogenase [46], and 3-phosphoglycerate kinase [45] and in the multi-tryptophan proteins lysozyme [55] and myosin S-1 (the isolated myosin head) [56]. Our findings are in essential agreement with all of these studies.

The width (FWHM) of a lifetime distribution corresponds to the density of states available to the emitting chromophores and has been associated with the degree of freedom of a fluorescent species in a given conformational space [26–28,57]. The bimodal analysis thus suggests that the two classes of fluorescent tryptophans in the rod correspond to two physically distinguishable populations. One is a long lifetime, red-shifted, solvent accessible species that is either immobile or rapidly moving within a homogeneous polar, probably aqueous, environment; the other is a short lifetime, solvent inaccessible species with blue-shifted emission spectrum that is either immobile and statically distributed among numerous heterogeneous nonpolar, probably protein, environments or is rapidly interconverting between them on the fluorescence time scale.

The assignment of these fluorescent species to particular tryptophans in the rod is problematic. There are two pairs of tryptophans (at positions 532 and 617) located at equivalent hydrophobic *d* sites in the heptad repeat (Fig. 6). Although arguments from structural symmetry would suggest that each tryptophan of a pair is in equivalent chemical and physical environments, this equivalence is questionable in a dimer made up of two flexible α-helices ≈ 1500 Å long entwined into a coiled-coil [3,58]. Recent NMR data indicate that some of the equivalent residues in the C-terminal of myosin rod are not in fact in chemically equivalent environments [59]. In principle, therefore, each of the four tryptophans in the rod could be in a distinct environment with complex (multi-exponential) excited state decay behavior. Given this possible physical complexity, it is the presence of a major species with a discrete long lifetime, rather than the distribution of short lifetimes, that requires explanation. Since there are no specific reasons to associate the measured lifetime species with specific tryptophans in the sequence, we refrain from doing so.

Another interpretation of the lifetime distributions is also possible. The different lifetime species may reflect different conformations of the protein, rather than different tryptophans within the protein. This analysis suggests that these different lifetime species may correspond to conformations in which the indole rings have differential solvent exposure. The long lifetime component could correspond to a conformation of the rod in which the indole side chain is partially exposed to aqueous solvent near the coiled-coil surface, and the short lifetime species could correspond to multiple protein conformations in which the indole rings are buried at the non-polar coiled-coil interface. Residues at hydrophobic *d* sites are known from crystallographic data [60] to form the structural interface of the coiled-coil, an arguably non-polar environment. The distribution of lifetime species would thus suggest that the bulky indole rings located at the hydrophobic *d* sites are actually in equilibrium between two distinct conformations, a polar conformation in contact with aqueous solvent and a non-polar conformation in contact with quenching groups in the protein; this equilibrium may apply to all four side chains in the sequence. The nature of this putative conformational equilibrium remains ambiguous.

An exact assignment of the physical origin of the observed lifetime distributions awaits further experiments. Studies of the tryptophan photophysics in single (pair) tryptophan mutants should shed considerable light on this issue.

Acknowledgements

This is publication number D-10115-1-93 of the New Jersey Agricultural Experiment Station. We are particularly grateful to Dr. Scott Williams of the Regional Laser and Biotechnology Lab for expert help in the data analysis. This work was supported in part by the State of New Jersey, by a Grant-in-Aid of Research from Sigma Xi, the Scientific Research Society (to Y-c.C.), and by NIH grant RR01348 to the Regional Laser and Biotechnology Laboratory.

References

1 R.D.B. Fraser and T.P. MacRae, Conformation in fibrous proteins. (Academic Press, New York, 1973).
2 C. Cohen and D.A.D. Parry, Proteins 7 (1990) 1.
3 S. Lowey, H.S. Slayter, A.G. Weeds, and H. Baker, J. Mol. Biol. 42 (1969) 1.
4 F.H.C. Crick, Acta Crystallogr. 6 (1953) 685.
5 D.A.D. Parry, in: Celluar and Molecular Biology of Intermediate Filaments. eds. R.D. Goldman and P.M. Steinert (Plenum Press, New York, 1990) p. 175.
6 S.L. McKnight, Sci. Am. 264 (1991) 54.
7 F.H.C. Crick, Acta Crystallogr. 6 (1953) 689.
8 A. Lupas, M. Van Dyke and J. Stock, Science 252 (1991) 1162.
9 A.D. McLachlan, Annu. Rev. Biophys. Bioeng. 13 (1984) 167.
10 W.F. Harrington and M.E. Rodgers, Annu. Rev. Biochem. 53 (1984) 35.
11 R.C. Lu and A. Wong, J. Biol. Chem. 260 (1985) 3456.
12 K. Maeda, G. Sczakiel, and A. Wittinghofer, Eur. J. Biochem. 167 (1987) 97.
13 H.E. Huxley, Science 164 (1969) 1356.
14 A.F. Huxley, Prog. Biophys. Chem. 7 (1957) 225.
15 A.G. Weeds and R.S. Taylor, Nature 257 (1975) 54.
16 L. King and S.S. Lehrer, Biochemistry 28 (1989) 3498.
17 Y.-c. Chang and R.D. Ludescher, Time-resolved laser spectroscopy in Biochemistry III. SPIE Proc. 1640 (1992) 159.
18 Y.-c. Chang and R.D. Ludescher, Biophys. J. 61 (1992) A180 (abstract).
19 D.D. Thomas, S. Ishiwata, J.C. Seidel and J. Gergely, Biophys. J. 32 (1980) 873.
20 T.M. Eads, D.D. Thomas and R.H. Austin, J. Molec. Biol. 178 (1984) 55.
21 W.F. Harrington and M. Burke, Biochemistry 11 (1972) 1448.
22 R.F. Chen, J. Res. Natl. Bur. Std. Sect. A. 76A (1972) 593.
23 J.R. Lakowicz, Principles of fluorescence spectroscopy (Plenum Press, New York, 1983).
24 J.M. Beechem, E. Gratton, M. Ameloot, J.R. Knutson and L. Brand, in: Topics in fluorescence spectroscopy, Vol 2, ed. J.R. Lakowicz (Plenum Press, New York, 1991) p. 241.
25 A. Grinvald and I.Z. Steinberg, Anal. Biochem. 59 (1974) 583.
26 J.R. Alcala, E. Gratton and F.G. Prendergast, Biophys. J. 51 (1987) 597.
27 J.R. Alcala, E. Gratton and F.G. Prendergast, Biophys. J. 51 (1987) 925.
28 R.D. Ludescher, J.J. Volwerk, G.H. de Haas and B.S. Hudson, Biochemistry 247 (1985) 240.
29 A.P. Demchenko, Ultraviolet spectroscopy of proteins (Springer-Verlag, Berlin. 1986).
30 E.A. Burstein, N.S. Vedenkina and M.N. Ivkova, Photochem. Photobiol. 18 (1973) 263.
31 D.B. Wetlaufer, Adv. Prot. Chem. 17 (1962) 303.
32 J. Eisinger, Biochemistry 8 (1969) 3902.
33 R.W. Cowgill, Biochim. Biophys. Acta 168 (1968) 431–438.
34 J.R. Lakowicz and G. Weber, Biophys. J. 32 (1980) 591.
35 A.P. Demchenko, Tr. Biochem. Sci. 13 (1988) 374.
36 T.Y. Tsong, T. Karr and W.F. Harrington, Proc. Natl. Acad. Sci., U.S.A. 76 (1979) 1109.
37 C.A. Swenson and P.A. Ritchie, Biochemistry 19 (1980) 5371.
38 I. Gonzalo and J.L. Escudero, J. Phys. Chem. 86 (1982) 2896.
39 A.P. Demchenko, Eur. Biophys. J. 16 (1988) 121–129.
40 A.P. Demchenko and A.S. Ladokhin, Biochim. Biophys. Acta 955 (1988) 352.
41 B. Valeur and G. Weber, Photochem. Photobiol. 25 (1977) 441.
42 S.V. Konev, Fluorescence and phosphorescence of proteins and nucleic acids (Plenum Press, New York, 1967).
43 K.K. Turoverov and I.M. Kuznetsova, Molekulyarnaya Biologiya (Russian) 19 (1985) 1321.
44 J.C. Brochon, P. Wahl, M. Charlier, J.C. Maurizot and C. Hélène, Biochem. Biophys. Res. Commun. 79 (1977) 1261.
45 J.P. Privat, P. Wahl, J.C. Auchet and R.H. Pain, Biophys. Chem. 11 (1980) 239.
46 J.B.A. Ross, C.J. Schmidt and L. Brand, Biochemistry 20 (1981) 4369.
47 Y.-c. Chang and R.D. Ludescher, Biophys. Chem. 48 (1993) 49.
48 G. Weber, Biochem. J. 75 (1960) 335.
49 J. Eisinger, B. Feuer and A.A. Lamola, Biochemistry 8 (1969) 3908.
50 Y. Saito, H. Tachibana, H. Hayaski and A. Wada, Photochem. Photobiol. 33 (1981) 289.
51 A.P. Demchenko and A.S. Ladokhin, Eur. Biophys. J. 15 (1988) 369.
52 J. Knutson, L. Davenport and L. Brand, Biochemistry 25 (1986) 1805.
53 D.A. Johnson and J. Yguerabide, Biophys. J. 48 (1985) 949.

54 J.P. Privat, P. Wahl and J.C. Auchet, Biophys. Chem. 9 (1979) 223.
55 C. Formoso and L.S. Forster, J. Biol. Chem. 250 (1975) 3738.
56 P.M. Torgerson, Biochemistry 23 (1984) 3002.
57 R.D. Ludescher, I.D. Johnson, J.J. Volwerk, G.H. de Haas, P.C. Jost and B.S. Hudson, Biochemistry 27 (1988) 6618.
58 C. Cohen, S. Lowey, R.G. Harrison, J. Kendrick-Jones and A.G. Szent-Gyorgi, J. Mol. Biol. 47 (1970) 605.
59 H.R. Kalbitzer, K. Maeda, A. Rosch, Y. Maeda, M. Geyer, W. Beneicke, K.P. Neidig and A. Wittinghofer, Biochemistry 30 (1991) 8083.
60 E.K. O'Shea, J.D. Klemm, P.S. Kim and T. Alber, Science 254 (1991) 539.